CHEMISTRY OF MATERIALS

Article

pubs.acs.org/cm

Thermal Atomic Layer Etching of ZnO by a "Conversion-Etch" Mechanism Using Sequential Exposures of Hydrogen Fluoride and Trimethylaluminum

David R. Zywotko[†] and Steven M. George*[,†,‡]

[†]Department of Chemistry and Biochemistry, [‡]Department of Mechanical Engineering, University of Colorado, Boulder, Colorado 80309-0215, United States

ABSTRACT: The atomic layer etching (ALE) of ZnO thin films was demonstrated using sequential, self-limiting thermal reactions with hydrogen fluoride (HF) and trimethylaluminum (TMA) as the reactants. The initial polycrystalline ZnO films were grown by atomic layer deposition (ALD) using diethylzinc (DEZ) and H_2O at 150 °C. The thermal ZnO ALE process was then studied between 205 and 295 °C using various techniques. *In situ* quartz crystal microbalance (QCM) measurements monitored ZnO ALE at 265 °C. The ZnO etching was linear versus number of ALE cycles. The HF exposure caused a mass gain of ΔM_{HF} = +53 ng/cm^2 from fluorination. The subsequent TMA exposure caused a large mass loss of ΔM_{TMA} = −172 ng/cm^2. This mass loss was much larger than expected from metal fluoride removal resulting from ligand-exchange transmetalation. The large mass loss suggested that there is a "conversion-etch" mechanism where TMA also converts the ZnO surface to an Al_2O_3 surface layer. This conversion reaction is believed to occur according to $3ZnO + 2Al(CH_3)_3 \rightarrow Al_2O_3 + 3Zn(CH_3)_2$. The ALE reaction would then proceed by $Al_2O_3 + 6HF + 4Al(CH_3)_3 \rightarrow 6AlF(CH_3)_2 + 3H_2O$. In this etching process, the Al_2O_3 layer is first fluorinated by HF to produce an AlF_3 surface layer. The AlF_3 surface layer is then removed by ligand-exchange transmetalation with TMA to yield volatile $AlF(CH_3)_2$ reaction products. After the AlF_3 removal, TMA then reacts with additional ZnO to regenerate the Al_2O_3 surface layer. The average mass change per cycle (MCPC) during ZnO ALE was −119 ng/cm^2 at 265 °C. This MCPC corresponds to an etch rate of 2.11 Å/cycle using a ZnO film density of 5.62 g/cm^3. The QCM measurements showed that the sequential HF and TMA reactions were self-limiting versus reactant exposure. *Ex situ* spectroscopic ellipsometry (SE) determined that the etch rates were temperature dependent, and the etch rates leveled off at higher temperatures. The etch rates ranged from 0.01 Å/cycle at 205 °C to 2.19 Å/cycle at 295 °C. Atomic force microscopy (AFM) measurements observed that the ZnO ALD films were smoothed by ZnO ALE. The conversion-etch mechanism may occur during the ALE of other metal compounds. This conversion-etch mechanism reaction may expand the number of materials that can be etched by thermal ALE methods.

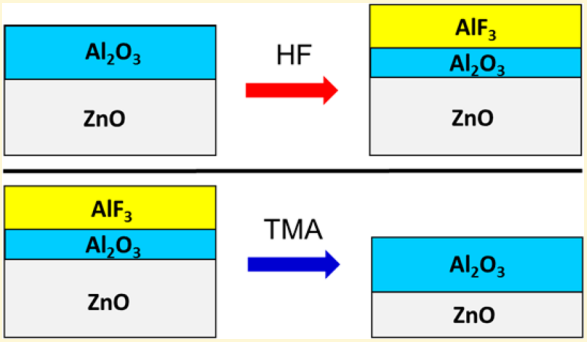

I. INTRODUCTION

Atomic layer processes such as atomic layer deposition (ALD)[1] and atomic layer etching (ALE)[2] are needed for the atomic level precision required to add or remove material to fabricate nanostructured devices.[3] Most reported ALE processes are based on halogenation reactions followed by energetic ion or noble gas atom bombardment to etch the material.[2,4,5] This ALE strategy has been demonstrated for Si,[6,7] Ge,[8] compound semiconductors,[9,10] metal oxides,[11−13] and carbon substrates.[14,15] Recently, new thermal ALE strategies have been developed on the basis of sequential fluorination and ligand-exchange reactions and applied for Al_2O_3 ALE,[16−18] HfO_2 ALE,[19] ZrO_2 ALE,[20] and AlN ALE.[21]

In the new thermal ALE method,[3,16,22] fluorination first converts the metal compound, such as a metal oxide or metal nitride, to a metal fluoride. Subsequently, a metal precursor undergoes a ligand-exchange transmetalation reaction[23] with the metal fluoride. During the ligand-exchange reaction, the metal precursor accepts fluorine from the metal fluoride and donates one of its ligands to the surface layer to produce volatile reaction products that lead to etching.[3,16,22] Hydrogen fluoride (HF) has been employed as the fluorination source. $Sn(acac)_2$ and trimethylaluminum (TMA) have been used as the metal precursor for ligand-exchange.[17,18] Other fluorination precursors, such as SF_4, and metal precursors, such as $AlCl(CH_3)_2$ and $SiCl_4$, can also be employed for thermal ALE.[20] The use of different fluorination and metal precursors provide pathways for selective thermal ALE.[20]

Although thermal ALE methods are promising, thermal ALE has been demonstrated for only a few metal compounds to date. In addition, most of these metal compounds have been grown using ALD methods and have been amorphous. In this

Received: October 22, 2016
Revised: January 5, 2017
Published: January 5, 2017

DOI: 10.1021/acs.chemmater.6b04529
Chem. Mater. 2017, 29, 1183−1191

paper, thermal ALE is examined for polycrystalline ZnO ALD films. ZnO is a wide-bandgap semiconductor that has many applications in various areas such as optoelectronics, surface acoustic wave devices, and transparent electronics.[24] Etching is required to fabricate ZnO devices. Earlier approaches for the dry etching of ZnO have focused on plasma etching using chlorine and hydrocarbon-based chemistries.[24−27] Thermal ZnO ALE methods can provide more control of the etching rates and also avoid plasma-induced damage during etching.[27]

ZnO ALE was studied by *in situ* quartz crystal microbalance (QCM) and *ex situ* spectroscopic ellipsometry (SE) measurements using HF and TMA as the reactants. The QCM and SE measurements examined the effect of various reaction conditions such as reactant exposure and temperature. The ZnO ALE etching rates were determined over the temperature range between 205 and 295 °C. The QCM investigations revealed large mass changes during the TMA exposures that were not consistent with only a ligand-exchange reaction. The large mass losses during the TMA exposures required an alternative etching mechanism based on both ligand-exchange and an additional conversion of ZnO to Al_2O_3. This new "conversion-etch" mechanism may occur frequently during metal precursor reactions and may allow a wide variety of additional materials to be etched using thermal ALE.

II. EXPERIMENTAL SECTION

II.A. Viscous Flow Hot-Wall Reactor with *in Situ* Quartz Crystal Microbalance. A hot-wall stainless steel reactor was utilized for the ALD growth and the subsequent ALE removal. The reactor was built in-house and adjusted for optimal viscous flow conditions.[28] The mass changes during ALD and ALE were monitored by an *in situ* quartz crystal microbalance.[28] The QCM sensor was a quartz crystal (gold coated, 6 MHz, 285 °C optimized, Inficon) mounted inside of a customized bakeable sensor housing (modified BSH-150, Inficon). The sensor housing was sealed using a low-outgassing, high temperature epoxy (Epo-Tek H21D, Epoxy Technology, Inc.). All of the QCM measurements were recorded by a thin film deposition monitor (Maxtek TM-400, Inficon). The mass sensitivity of the Maxtek monitor was ∼0.375 ng/cm^2.

The reactor temperature was held constant to ±0.1 °C by a proportional-integral-derivative (PID) temperature controller (2408, Eurotherm) and power controller (7100A, Eurotherm). These controllers operated two ceramic fiber heaters (VS102A06S, VS102A12S, Watlow) that encased the reactor body. The isothermal environment is important for high quality QCM measurements. After loading the QCM, or changing operation temperatures, the reactor was allowed to reach its new equilibration conditions over the course of 4 h.

The reactor was equipped with a corrosion-resistant, two-stage rotary vane pump (Pascal 2010C1, Pfeiffer). A bakeable capacitance manometer (Baratron 121A, MKS) was used to monitor the pressure inside the reactor. The pump was able to maintain a base pressure of ∼20 mTorr without any N_2 flow. Under experimental conditions, three mass flow controllers provided a constant flow of 170 sccm of ultrahigh purity (UHP) N_2 gas (99.999%, Airgas) through the reactor. Two mass flow controllers (1179A, MKS) controlled the N_2 flow through the metal and nonmetal precursor lines. Each line had a constant flow of 75 sccm that purged the precursor zones and subsequently entered the main chamber. An additional mass flow controller (1159B, MKS) provided a steady flow of 20 sccm through the QCM housing underneath the crystal to prevent backside deposition. The total N_2 flow of 170 sccm maintained an experimental pressure of ∼1.2 Torr in the chamber.

Prior to each ALE experiment, fresh substrate films were grown on the *in situ* QCM crystal at 150 °C. An Al_2O_3 ALD layer with a thickness of ∼5 nm was deposited initially to aid ZnO ALD nucleation. The Al_2O_3 was deposited using 50 cycles of TMA (97%, Sigma-Aldrich) and H_2O (HPLC grade, submicron filtered, Fisher Scientific) as the reactants. Subsequently, a ZnO ALD layer with a thickness of ∼80 nm was deposited using 400 cycles of diethylzinc (DEZ; 52 wt % Zn, Sigma-Aldrich) and H_2O as the reactants. All ALD reagents were held at room temperature. ZnO ALD films were also deposited on Si(100) witness wafers. The thickness of these ZnO ALD films was measured using SE. In agreement with earlier studies,[29] the ZnO ALD growth rate was 2.0 Å/cycle.

The ZnO ALE experiments using the QCM were performed at 265 °C. Controlled etching was accomplished by sequential exposures of HF, originating from HF-pyridine (70 wt % HF, Sigma-Aldrich), and TMA. HF-pyridine is a convenient liquid source of HF. The HF vapor pressure above this solution is 90−100 Torr at room temperature.[19] There is negligible pyridine vapor pressure above the HF-pyridine solution.[30] The HF-pyridine was transferred to a gold-coated stainless steel bubbler in a dry, N_2 purged glovebag. The HF-pyridine underwent freeze−pump−thaw cycles to eliminate dissolved gases. Both the HF-pyridine and TMA doses were controlled by two pneumatically actuated valves in combination with a metering valve. The HF-pyridine and TMA precursor doses produced consistent pressure transients of ∼60 and ∼80 mTorr, respectively. Both ALE reactants were held at room temperature.

II.B. ALD and ALE on Silicon Wafers for *ex Situ* Film Analysis. The *ex situ* studies of ZnO deposition and etching were performed on boron-doped Si wafers (p-type, ⟨100⟩, Silicon Valley Microelectronics). The 125 mm Si wafers were cleaved into 2 cm by 2 cm squares and then rinsed with deionized water, acetone, and methanol. UHP N_2 was used to blow dry the samples. The samples were loaded into the reactor and given a minimum of 2 h for thermal equilibration. After deposition of the Al_2O_3 ALD nucleation layer and the ZnO ALD film at 150 °C, the samples were removed from the reactor for the *ex situ* SE thickness measurements. The samples were then rinsed with methanol, blown dry with UHP N_2, and reinserted into the reactor for the ALE experiments. ZnO ALE experiments were performed between 205 and 295 °C.

The crystallinity of the ZnO substrates was confirmed using a high resolution grazing-incidence X-ray diffractometer (XRD) (Bede D1, Jordan Valley Semiconductors) with Cu Kα radiation at 1.540 Å. Scans were performed from 20° to 80° with a step size of 0.05° and 50 s acquisition time. The filament voltage and current for the X-ray source were 40 kV and 35 mA, respectively. XRD software (QuickGraph 2.1.12, Jordan Valley Semiconductors) was used to analyze the data.

SE measurements were utilized to measure the thickness of the films after the ALD and ALE processes. A spectroscopic ellipsometer (M-2000UI, J.A. Woollam Co.) collected data between 245 and 1690 nm at angles of 65° and 75°. The CompleteEASE software, provided by J.A. Woollam Co., fitted the amplitude ratio (ψ) and phase difference (Δ) based on a custom model to determine the film thickness and index of refraction. The model accuracy was verified by thickness comparison with X-ray reflectometry measurements (Bede D1, Jordan Valley Microelectronics).

X-ray photoelectron spectroscopy (XPS) measurements were performed for elemental analysis of the sample surface. An X-ray photoelectron spectrometer (PHI 5600) recorded surface survey scans using monochromatic Al Kα radiation (E = 1486 eV). The XPS data were collected using AugerScan (RBD Instruments) and analyzed using CASA XPS software (Casa Software Ltd.). Atomic force microscopy (AFM) images were obtained using an easyScan 2 (Nanosurf) with a dynamic module. The data were collected using easyScan 2 AFM software (Nanosurf) and analyzed with Gwyddion.[31] The instrument utilized 1 μm × 1 μm scans for RMS surface roughness analysis before and after ZnO ALE.

III. RESULTS AND DISCUSSION

III.A. Initial ZnO ALD Film and *in Situ* Quartz Crystal Microbalance Studies. The initial ZnO ALD films on the silicon wafers were analyzed using XRD. Figure 1a shows an XRD scan of a ZnO film grown on a Si(100) wafer using 400 cycles of DEZ and H_2O exposures at 150 °C. This ZnO ALD

DOI: 10.1021/acs.chemmater.6b04529
Chem. Mater. 2017, 29, 1183−1191

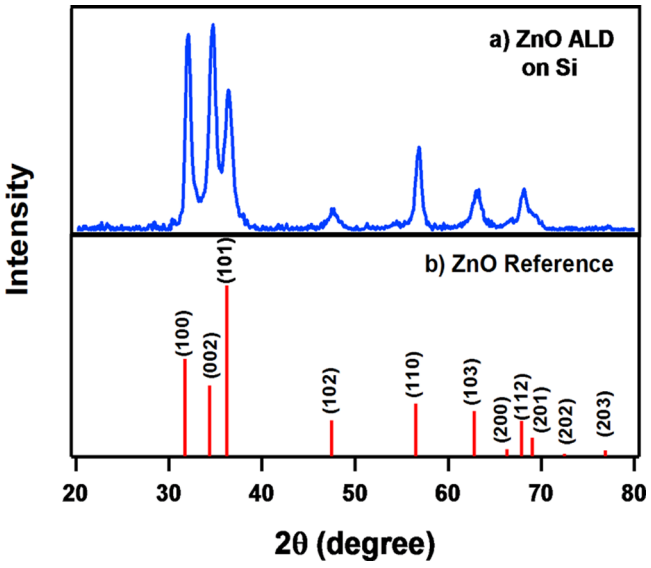

Figure 1. (a) Grazing incidence XRD spectrum for the ZnO substrate grown using 400 cycles of ZnO ALD at 150°C on a Si (100) wafer. (b) Reference XRD spectrum for crystalline (wurtzite) ZnO.

film had a thickness of ~80 nm. The XRD peaks reveal the film as polycrystalline ZnO.[32] Figure 1b shows the hexagonal wurtzite ZnO reference spectrum (ICDD-PDF Card # 89-1397). The intensities of the (002) and (101) peaks, at 34.65° and 36.30°, respectively, differ from the reference spectrum. This difference is characteristic of ZnO ALD films grown at 150 °C using DEZ and H_2O.[33]

The crystalline ZnO ALD films were then employed for the ZnO ALE experiments. Figure 2 shows the QCM mass change

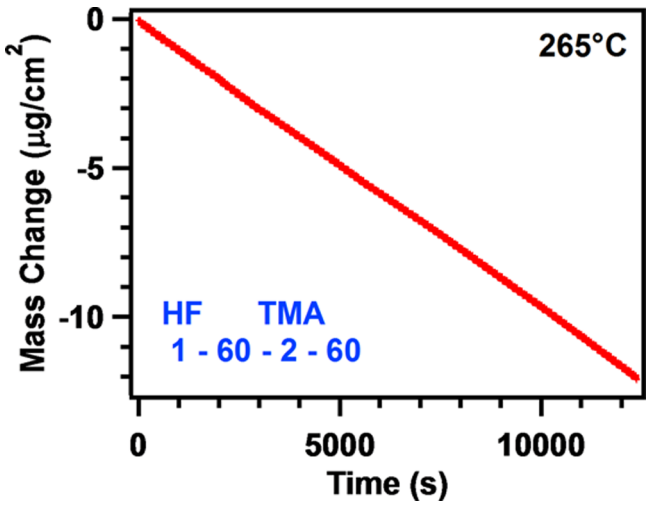

Figure 2. Mass change versus time for ZnO ALE using sequential exposures of HF and TMA at 265 °C.

versus time for 100 ALE cycles of sequential HF and TMA exposures on the ZnO ALD film at 265 °C. The ZnO ALE is performed using an HF exposure of 1 s, a N_2 purge of 60 s, a TMA exposure of 2 s, and last another N_2 purge of 60 s. This reaction sequence is represented as 1−60−2−60. The HF and TMA exposures during ZnO ALE produced pressure transients of ~60 and ~80 mTorr, respectively. The results for the mass change versus time in Figure 2 show linear etching of the ZnO film with an average mass change per cycle (MCPC) of −119 ng/cm^2. This MCPC is consistent with an etch rate of 2.11 Å/cycle using the ZnO ALD film density of 5.62 g/cm^3 determined by XRR analysis.

Figure 3 shows an expansion of the QCM results in Figure 2 for three cycles of HF and TMA exposures at 265 °C. The mass

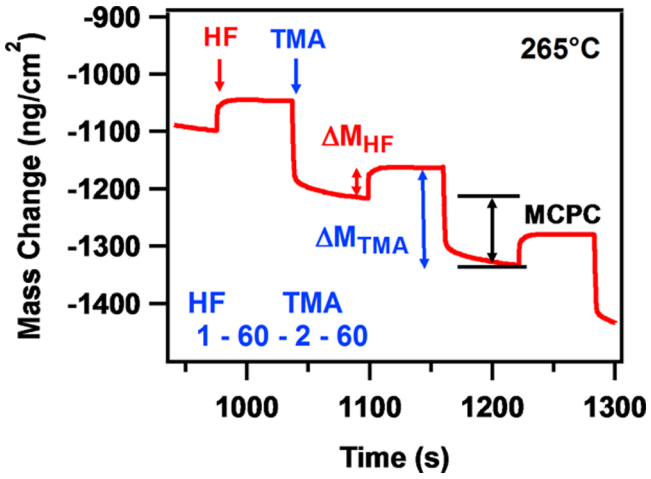

Figure 3. Expanded segment of Figure 2 showing mass changes during ZnO ALE using sequential exposures of HF and TMA at 265 °C. The ΔM_{HF} and ΔM_{TMA} mass changes are associated with individual exposures of HF and TMA. The MCPC is the sum of ΔM_{HF} and ΔM_{TMA}.

changes for the individual HF and TMA exposures are denoted ΔM_{HF} and ΔM_{TMA}, respectively. Figure 4 shows the ΔM_{HF} and

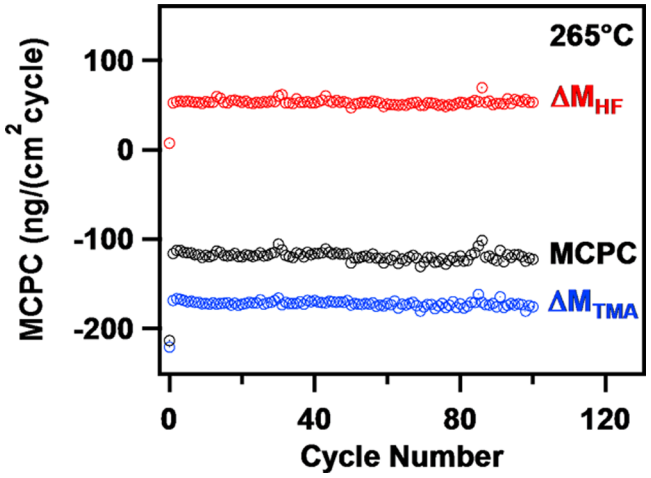

Figure 4. Mass changes during individual HF exposures (ΔM_{HF}), TMA exposures (ΔM_{TMA}), and the total mass change per cycle (MCPC) for ZnO ALE at 265 °C.

ΔM_{TMA} mass changes and the mass change per cycle (MCPC) versus cycle number for the 100 ALE cycles in Figure 2. The MCPC is defined as MCPC = ΔM_{HF} + ΔM_{TMA}. The ΔM_{HF} and ΔM_{TMA} mass changes and the MCPC are constant throughout the 100 ALE cycles at +53, −172, and −119 ng/cm^2, respectively. The mass changes for the first ZnO ALE cycle are different from the subsequent cycles. For the first cycle, the mass changes are ΔM_{HF} = +7.5 ng/cm^2 and ΔM_{TMA} = −221 ng/cm^2.

DOI: 10.1021/acs.chemmater.6b04529
Chem. Mater. 2017, 29, 1183−1191

The mass gain of ΔM_{HF} = +7.5 ng/cm^2 on the first HF exposure is attributed to fluorination of the ZnO surface given by

$$ZnO + 2HF \rightarrow ZnF_2 + H_2O \quad (1)$$

This fluorination reaction is favorable at 265 °C with ΔG = −9.6 kcal/mol.[34] ZnF_2 is a stable solid with a melting point of 872 °C.[35] The mass gain of +7.5 ng/cm^2 is possible by the fluorination of 2.05 × 10^{14} ZnO units/cm^2 to 2.05 × 10^{14} ZnF_2 units/cm^2 on the surface. The 2.05 × 10^{14} ZnF_2 units/cm^2 represents a thickness of 0.71 Å assuming a continuous and conformal ZnF_2 surface layer with a ZnF_2 density of 4.95 g/cm^3.

The first TMA exposure is then believed to lead to a ligand-exchange transmetalation reaction between TMA and ZnF_2. This ligand-exchange reaction would form volatile $AlF(CH_3)_2$ and $Zn(CH_3)_2$ reaction products.[3,17,18] The ligand-exchange reaction can be written as

$$ZnF_2 + 2Al(CH_3)_3(g) \rightarrow 2AlF(CH_3)_2(g) + Zn(CH_3)_2(g) \quad (2)$$

$Zn(CH_3)_2$ is a highly volatile compound with a vapor pressure of 15 Torr at 20 °C.[36] Assuming that this ligand-exchange reaction removes the entire ZnF_2 surface layer of 2.05 × 10^{14} ZnF_2 units/cm^2, the ligand-exchange reaction would only produce a small mass loss of −35.2 ng/cm^2. However, the mass loss during the first TMA reaction is much larger at ΔM_{TMA} = −221 ng/cm^2. This large mass loss suggests that an additional reaction must be occurring after the removal of the ZnF_2 surface layer.

The large mass loss is believed to occur by reaction between TMA and the underlying ZnO film. This reaction converts ZnO to Al_2O_3 according to

$$3ZnO + 2Al(CH_3)_3 \rightarrow Al_2O_3 + 3Zn(CH_3)_2 \quad (3)$$

This conversion reaction is thermochemically favorable with a Gibbs free energy change of ΔG = −166.8 kcal/mol at 265 °C.[34] The amount of ZnO converted to Al_2O_3 can be determined by assuming that the conversion reaction accounts for the difference between −221 and −35.2 ng/cm^2. The difference of −185.8 ng/cm^2 is consistent with the conversion of 23.6 × 10^{14} ZnO units/cm^2 to 7.86 × 10^{14} Al_2O_3 units/cm^2 on the surface. The 7.86 × 10^{14} Al_2O_3 units/cm^2 represents a thickness of 3.37 Å assuming a continuous and conformal Al_2O_3 surface layer with an Al_2O_3 density of 3.95 g/cm^3.

Evidence for the conversion of ZnO to Al_2O_3 was observed earlier during the growth of ZnO/Al_2O_3 alloy films using DEZ, TMA, and H_2O at 177 °C.[29] In these studies, QCM studies observed large mass losses during the first TMA exposure after ZnO ALD. This mass loss was interpreted as resulting in part from the surface reaction:

$$ZnOH^* + Al(CH_3)_3 \rightarrow Al(OH)(CH_3)^* + Zn(CH_3)_2 \quad (4)$$

where the astericks indicate the surface species.[29] Mass spectrometry studies subsequently confirmed the production of $Zn(CH_3)_2$ during TMA exposures that followed DEZ exposures during the growth of ZnO striped structures in porous substrates.[37] More recent QCM experiments have also documented the mass loss caused by the TMA exposure after DEZ exposures during the growth of Al-doped ZnO.[38]

After the first ALE cycle, Figure 4 shows that the next HF exposure and subsequent HF exposures yield a mass gain of ΔM_{HF} = +53 ng/cm^2. This mass gain is attributed to the fluorination of the Al_2O_3 surface layer to AlF_3. The next TMA exposure and subsequent TMA exposures then produce a mass loss of −172 ng/cm^2. This mass loss can be explained by the removal of the AlF_3 layer by the ligand-exchange reaction and an additional conversion reaction of ZnO to Al_2O_3. A complete discussion of these mass changes and comparison with the measured ZnO etch rates will be given later in Section III.C.

The self-limiting nature of the ZnO ALE process is characterized in Figure 5. The MCPC for ZnO ALE is

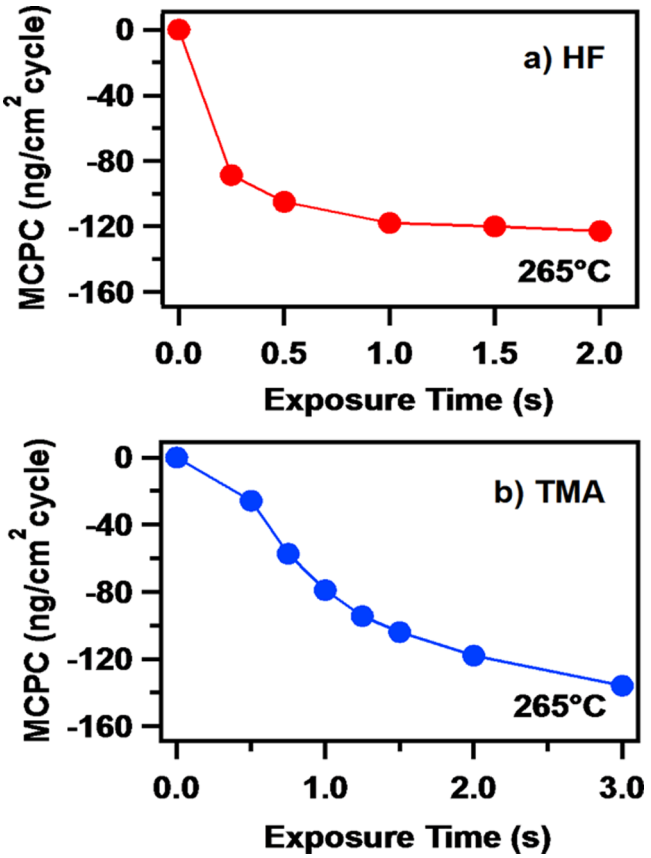

Figure 5. Mass change per cycle (MCPC) at 265 °C versus precursor exposure time for (a) HF exposure with TMA exposure fixed at 2 s and (b) TMA exposure with HF exposure fixed at 1s.

examined while changing the exposure time of one precursor and holding the exposure time of the other precursor constant. In Figure 5a, the HF exposure is varied while the TMA exposure is fixed at 2 s. This sequence is denoted as x−60−2−60, where a N_2 purge of 60 s is used after each exposure. As the HF exposure is increased, the MCPC decreases and then levels off at −119 ng/(cm^2 cycle). This leveling off is an indication that the fluorination reaction exhibits self-limiting behavior. Figure 5a indicates that a HF exposure of 1 s is sufficient for the saturation of the HF reaction.

Figure 5b analyzes the self-limiting nature of the TMA reaction during ZnO ALE. The TMA exposure is varied while the HF exposure is held at 1 s. This sequence is designated as 1−60−x−60 sequence. The MCPC displays nearly self-limiting behavior. The MCPC drops slightly from −119 ng/(cm^2 cycle) at a 2 s TMA exposure to −138 ng/(cm^2 cycle) at a 3 s TMA exposure. This additional mass loss may be associated with the conversion of additional ZnO to Al_2O_3 at larger TMA

DOI: 10.1021/acs.chemmater.6b04529
Chem. Mater. 2017, 29, 1183−1191

exposures. More converted ZnO to Al_2O_3 could in turn lead to thicker AlF_3 layers after fluorination and then more etching during the ligand-exchange reaction.

The self-limiting nature of the fluorination reaction can be explained by the formation of a passivating fluoride layer during the HF exposure. The passivating surface layer can be understood if the fluoride layer forms a diffusion barrier on the metal oxide analogous to metal oxides on metals[39,40] or SiO_2 layers on silicon.[41,42] The self-limiting nature of the TMA ligand-exchange and conversion reaction may also result from the Al_2O_3 layer forming a diffusion barrier on ZnO. The Al_2O_3 layer may impede the diffusion kinetics required for additional conversion of ZnO to Al_2O_3.

The passivating fluoride layer can also be explained using the Pilling-Bedworth ratio (R_{PB}). R_{PB} is defined as the ratio of the molar volume, V, of the top layer to the molar volume of the underlying material.[43] Systems with $R_{PB} > 1$ can form passivating top layers because of compressive stress in the top layer.[44] The molar volume for AlF_3 is V_{AlF3} = 28.96 cm^3/mol based on M_{AlF3} = 83.98 g/mol and ρ_{AlF3} = 2.9 g/cm^3.[30] The molar volume for Al_2O_3 is V_{Al2O3} = 32.89 cm^3/mol based on M_{Al2O3} = 101.96 g/mol and ρ_{Al2O3} = 3.1 g/cm^3. The fluorination of Al_2O_3 to AlF_3 is expected to self-passivate because $R_{PB} = (2 \times V_{AlF3})/V_{Al2O3} = 1.76$. The coefficient of 2 is added for proper reaction stoichiometry.

QCM results for pulse sequences with exposures that have not reached completion for both reactants can also display a linear mass loss versus HF and TMA exposures. Figure 6

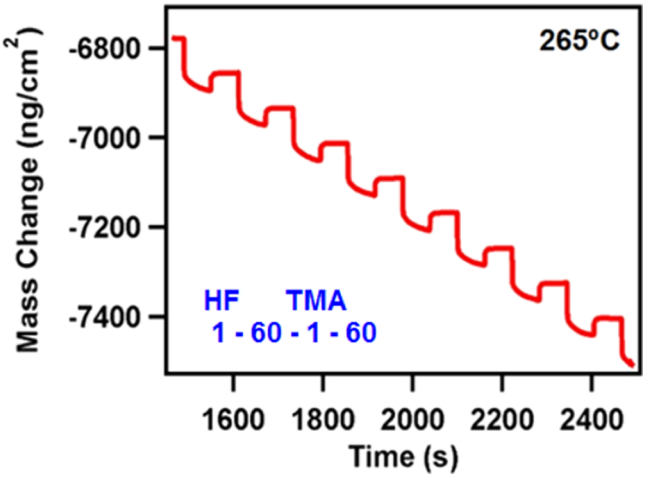

Figure 6. Mass change versus time for ZnO ALE at 265 °C under sub-self-limiting conditions as determined by Figure 5 using a 1 s exposure of HF and a 1 s exposure of TMA.

displays mass change versus time obtained during a 1−60−1−60 pulse sequence at 265 °C. In these experiments, the TMA reaction does not go to completion according to Figure 5b. The HF exposure of 1 s is sufficient for the HF reaction to reach completion. Although the TMA reaction does not reach completion, these results still exhibit a linear mass loss versus HF and TMA exposures. This behavior indicates that the etch rate for ZnO ALE could be lowered by operating the reactions in the subsaturation regime. However, the resulting etched ZnO films may not be as smooth as the ZnO films etched using reactant exposures that are self-limiting.

III.B. SE, AFM, and XPS Measurements. SE measurements examined the thickness change after various numbers of ZnO ALE cycles on ZnO ALD films. The ZnO films were grown by 400 cycles of ZnO ALD on Si(100) wafers at 150 °C. Figure 7 shows thickness change versus number of ALE cycles

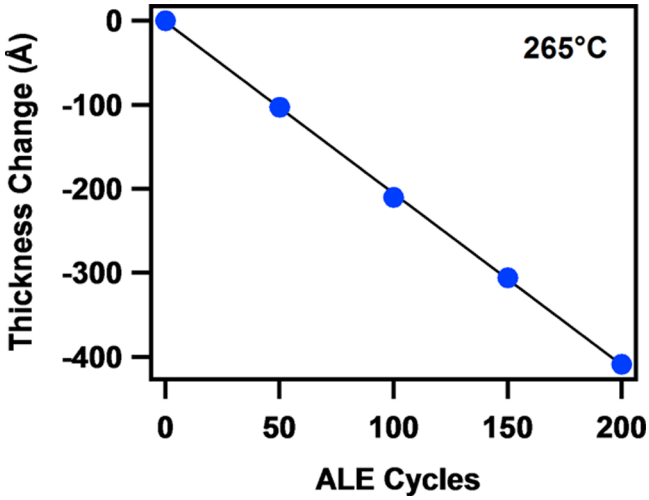

Figure 7. Thickness change of the ZnO film versus number of ZnO ALE cycles at 265 °C determined by spectroscopic ellipsometry measurements.

for ZnO films at 265 °C. Thickness changes of −103, −211, −306, and −409 Å were observed after 50, 100, 150, and 200 cycles of ZnO ALE, respectively. These measurements yield an etch rate of 2.05 Å/cycle at 265 °C. This etch rate is in excellent agreement with the etch rate of 2.11 Å/cycle at 265 °C obtained from the QCM measurements.

Atomic force microscopy (AFM) imaging was used to analyze the effect of ALE on the surface roughness. AFM measurements over 1 μm × 1 μm areas were performed first on the as-deposited ZnO ALD film and then again after 200 cycles of ZnO ALE at 265 °C. The polycrystalline ZnO ALD films have a surface roughness that increases with the number of ZnO ALD cycles used to deposit the film.[45] Prior to etching, the polycrystalline ZnO films had an RMS roughness of 11 Å. After 200 cycles of ZnO ALE, the RMS roughness was reduced to 5.8 Å. These results indicate the surface of the ZnO ALD film is smoothed by ZnO ALE. The smoothing of Al_2O_3 and HfO_2 substrates has also been observed for Al_2O_3 and HfO_2 ALE.[18,19]

Figure 8 displays the thickness change versus number of ZnO ALE cycles for temperatures between 205 and 295 °C. The reduction of the film thickness is linear versus number of ALE cycles at the various temperatures. The ZnO etch rates were 0.01, 1.07, 1.82, 2.05, and 2.19 Å/cycle for ALE temperatures 205, 220, 235, 265, and 295 °C, respectively. These results indicate that the ZnO etch rates can be tuned by adjusting the temperature.

Figure 9 displays the etch rate for ZnO ALE versus ALE temperature. The ZnO etch rates increase as the ALE temperature increases. The etch rates range from 0.01 Å/cycle at 205 °C to 2.19 Å/cycle at 295 °C. The leveling off of the ZnO etch rate at higher temperatures is believed to result from the TMA reaction. Fluorination of Al_2O_3 may not be dependent on temperature as shown earlier in the study of Al_2O_3 ALE using HF and TMA.[17] The increase in the ZnO etch rate from 205 to 235 °C is probably caused by the increasing efficiency for TMA reacting with AlF_3 and then

DOI: 10.1021/acs.chemmater.6b04529
Chem. Mater. 2017, 29, 1183−1191

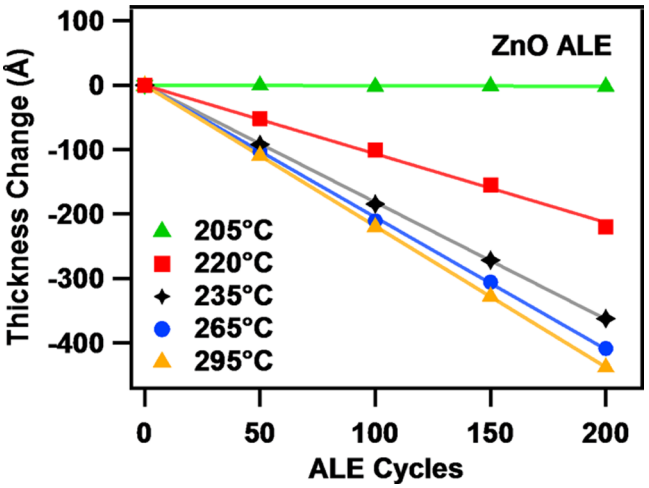

Figure 8. Spectroscopic ellipsometry measurements of the thickness change of the ZnO film versus number of ZnO ALE cycles at a variety of temperatures between 205 and 295 °C.

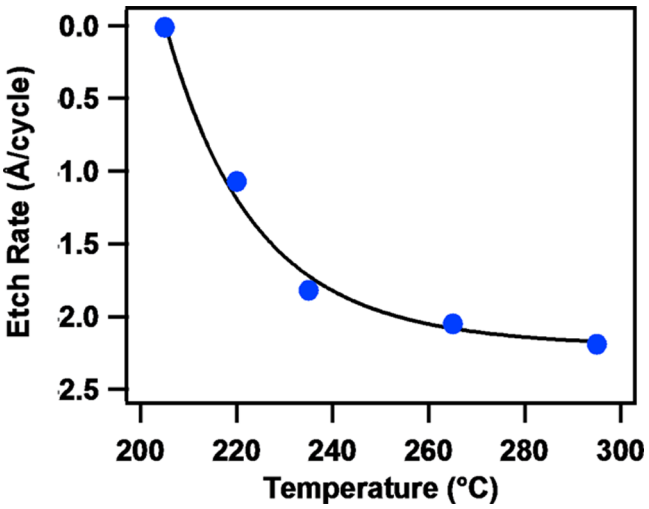

Figure 9. Temperature dependence of the ZnO etch rate between 205 and 295 °C.

converting ZnO to Al_2O_3. From 235 to 295 °C, there is a very slow increase in etch rate. This behavior would be expected if the TMA conversion reaction becomes limited by the Al_2O_3 passivation layer on ZnO.

X-ray photoelectron spectroscopy (XPS) measurements analyzed the elemental composition of the films before and after the ALE process. The samples were exposed to atmosphere while transferring to the XPS instrument. Prior to ZnO ALE, the XPS spectra from the ZnO ALD films monitored photoelectrons from Zn, O, and adventitious carbon. After 200 cycles of ALE at 265 °C ending with an HF exposure, the XPS results measured Al concentrations of 6.8 at% and F concentrations of 3.4 at%. These concentrations were quantified with adventitious carbon included in the list of elements summing to 100 at%. The XPS measurements confirm the presence of Al in the ZnO films.

The SE measurements also obtained the index of refraction, *n*, for the ZnO films before and after the ZnO ALE. For the as-prepared ZnO ALD films, the refractive index, *n*, was 1.96. For the Al_2O_3 ALD films grown in the same reactor at 150 °C, the refractive index, *n*, was 1.65. These refractive index values are consistent with earlier reported values.[46,47] In contrast, the refractive index for the ZnO films after 200 ALE cycles was 1.92. This lower refractive index is consistent with the incorporation of a lower refractive index material, such as Al_2O_3, in the ZnO film.

III.C. Proposed Mechanism of ZnO ALE. In the proposed reaction mechanism for ZnO ALE, the first HF exposure fluorinates the ZnO surface and produces a ZnF_2 surface layer as defined by eq 1. The first exposure of TMA then undergoes a ligand-exchange reaction with the ZnF_2 surface layer according to eq 2. The large mass change during the TMA exposure also indicates that TMA can continue to react with ZnO to form Al_2O_3 as described by eq 3. After the Al_2O_3 layer is established on the ZnO film, the etching reaction can occur as

$$Al_2O_3 + 6HF(g) + 4Al(CH_3)_3(g) \rightarrow 6AlF(CH_3)_2 + H_2O \quad (5)$$

The etching reaction given in eq 5 can be broken into fluorination and ligand-exchange reactions as follows:

$$Al_2O_3|Al_2O_3{}^* + 6HF(g) \rightarrow Al_2O_3|2AlF_3{}^* + 3H_2O(g) \quad (6)$$

$$Al_2O_3|2AlF_3{}^* + 4Al(CH_3)_3(g) \rightarrow Al_2O_3{}^* + 6AlF(CH_3)_2(g) \quad (7)$$

In eq 6, the Al_2O_3 surface layer is fluorinated by HF to form AlF_3 as illustrated in Figure 10a. This reaction is highly favorable with $\Delta G = -52.4$ kcal/mol at 265 °C.[34] This reaction also releases H_2O as a reaction product. HF reacting with any methylated surface species, $AlCH_3$*, also forms AlF_3 and releases CH_4 as a reaction product. The AlF_3 surface layer should be stable because AlF_3 has a high melting point of 1291 °C.[35]

In eq 7, the AlF_3 surface layer is removed by TMA through a ligand-exchange reaction as shown in Figure 10b. Previous studies have observed the spontaneous etching of AlF_3 films by $Al(CH_3)_3$ exposures at 300 °C.[30] This reaction would release $AlF(CH_3)_2$ as a volatile reaction product. The volatility of $AlF(CH_3)_2$ leads to mass loss and reduction of the film thickness. Loss of the AlF_3 layer also allows TMA to convert more ZnO to Al_2O_3 as illustrated in Figure 10c. The reaction of TMA with the Al_2O_3 surface also produces $AlCH_3$* surface species.

Figure 4 shows that the ΔM_{HF} and ΔM_{TMA} mass changes and the MCPC are constant throughout the 100 ALE cycles at 265 °C after the first ALE cycle. ΔM_{HF}, ΔM_{TMA}, and MCPC are +53, −172, and −119 ng/cm^2, respectively. The MCPC of −119 ng/cm^2 is consistent with a ZnO etch rate of 2.11 Å/cycle. The SE measurements independently yielded an etch rate of 2.05 Å/cycle at 265 °C. These mass changes and the ZnO etch rate can be employed to quantify the reactions during ZnO ALE after the first ALE cycle.

The constant mass gain of ΔM_{HF} = +53 ng/cm^2 resulting from the HF exposure is in agreement with the fluorination of 4.84×10^{14} Al_2O_3 units/cm^2 to 9.67×10^{14} AlF_3 units/cm^2 on the surface. Assuming continuous and conformal layers, the 4.84×10^{14} Al_2O_3 units/cm^2 represents an Al_2O_3 thickness of 2.07 Å based on an Al_2O_3 density of 3.95 g/cm^3. Likewise, the 9.67×10^{14} AlF_3 units/cm^2 represents an AlF_3 thickness of 4.68 Å based on an AlF_3 density of 2.88 g/cm^3.

Eq 3 can be employed to determine the number of ZnO units/cm^2 that are necessary to produce the 4.84×10^{14} Al_2O_3 units/cm^2. Given the reaction stoichiometry, 14.52×10^{14} ZnO

DOI: 10.1021/acs.chemmater.6b04529
Chem. Mater. 2017, 29, 1183−1191

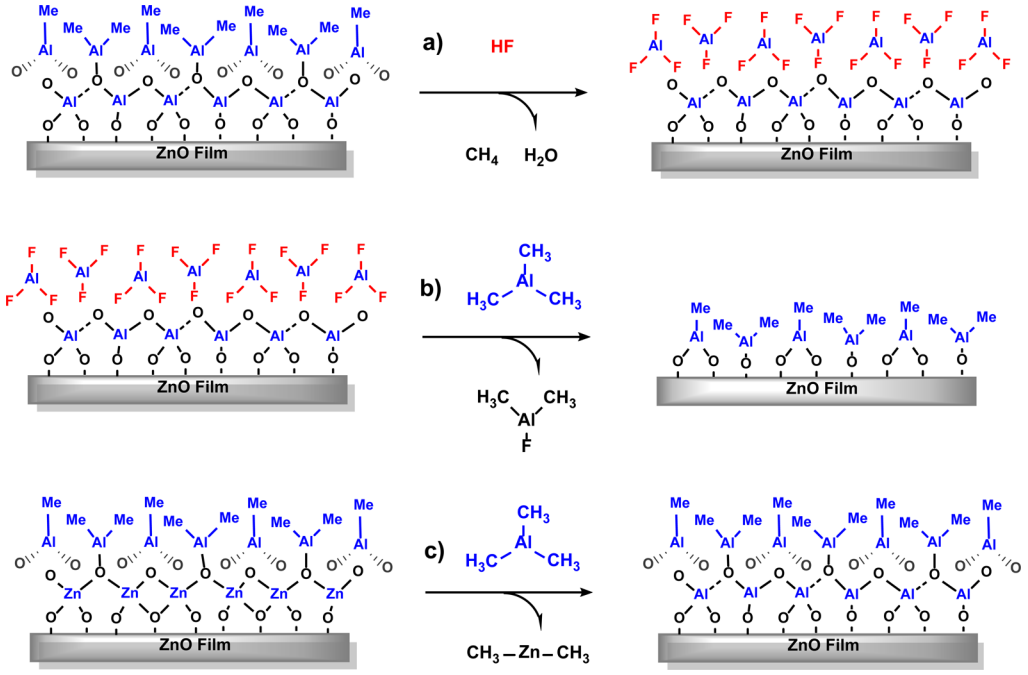

Figure 10. Mechanism of ZnO ALE using sequential HF and TMA exposures showing (a) fluorination reaction with HF; (b) ligand-exchange reaction with TMA; (c) conversion reaction of ZnO to Al_2O_3 with TMA.

units/cm^2 are required to form the 4.84 × 10^{14} Al_2O_3 units/cm^2. However, 14.52 × 10^{14} ZnO units/cm^2 is more than the ZnO etch rate of 2.11 Å/cycle. The ZnO etch rate of 2.11 Å/cycle represents only 8.77 × 10^{14} ZnO units/cm^2 using a ZnO density of 5.62 g/cm^3. The conversion of 8.77 × 10^{14} ZnO units/cm^2 would form 2.92 × 10^{14} Al_2O_3 units/cm^2. Assuming a continuous and conformal Al_2O_3 layer, this Al_2O_3 coverage represents a Al_2O_3 layer thickness of 1.25 Å.

To resolve this discrepancy between the ZnO etch rate and number of Al_2O_3 units/cm^2 needed to be converted to AlF_3 to produce the mass change of +53 ng/cm^2, more Al_2O_3 is required from another source in addition to the ZnO conversion reaction. This extra Al_2O_3 may result from the reaction of TMA with residual H_2O or surface hydroxyl groups. The residual H_2O may be produced by the previous HF exposure. To obtain 4.84 × 10^{14} Al_2O_3 units/cm^2, the extra Al_2O_3 from TMA reactions with H_2O or hydroxyl groups is 1.92 × 10^{14} Al_2O_3 units/cm^2. This extra Al_2O_3 represents a Al_2O_3 layer thickness of 0.82 Å assuming a continuous and conformal Al_2O_3 layer.

To present a visual representation of the "conversion-etch" mechanism, Figure 11 summarizes the surface reactions and film thicknesses during ZnO ALE for the first ALE cycle and subsequent ALE cycles at 265 °C. The first HF exposure on ZnO is shown in Figure 11a. This HF exposure produces a ZnF_2 surface layer with a thickness of 0.71 Å. The first TMA exposure is given in Figure 11b. This TMA exposure removes the ZnF_2 layer. In addition, the TMA exposure converts ZnO to Al_2O_3 and produces an Al_2O_3 layer thickness of 3.37 Å.

The next and subsequent HF exposures on Al_2O_3 are displayed in Figure 11c. These HF exposures yield AlF_3 layers with a thickness of 4.68 Å. The remaining Al_2O_3 underneath this AlF_3 layer would have a thickness of 1.30 Å. This Al_2O_3 ALD thickness assumes that the TMA exposures from subsequent cycles produce Al_2O_3 thicknesses equivalent to the first ALE cycle. The next and subsequent TMA exposures

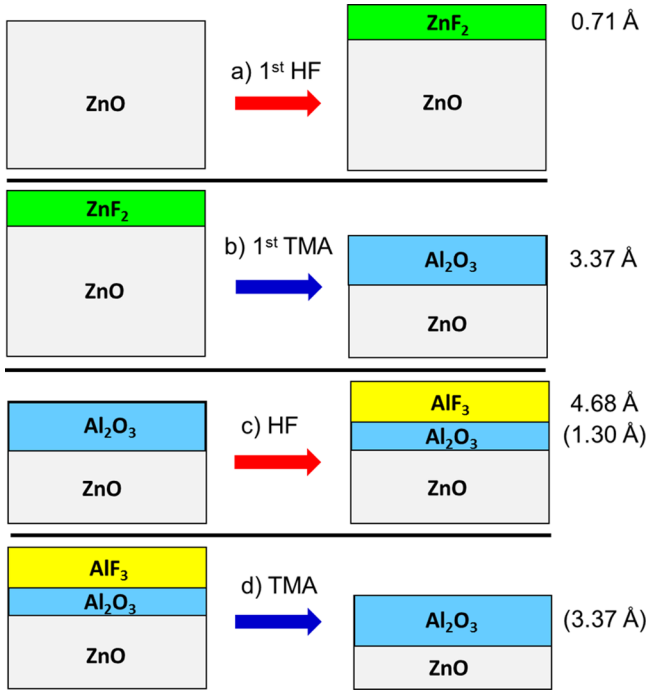

Figure 11. Schematic of the surface layers and layer thicknesses resulting from the sequential HF and TMA exposures during the first ZnO ALE cycle and subsequent ZnO ALE cycles at 265 °C.

illustrated in Figure 11d would then remove the AlF_3 layer and add an Al_2O_3 layer thickness of 2.07 Å by the conversion of ZnO to Al_2O_3 and reaction with residual H_2O or hydroxyl groups. The resulting Al_2O_3 layer thickness is 3.37 Å to agree with the Al_2O_3 layer thickness produced in the first ALE cycle.

III.D. Generality of Conversion-Etch Mechanism. The conversion of ZnO to Al_2O_3 in the reaction mechanism for ZnO ALE may be a fairly general phenomena. The conversion

DOI: 10.1021/acs.chemmater.6b04529
Chem. Mater. 2017, 29, 1183−1191

reaction is driven by the stability of the product metal oxide. The conversion reaction can be expected when the metal precursor can form a metal oxide that is more stable than the initial metal oxide. When using TMA as the metal precursor, the conversion reaction is very likely because Al_2O_3 is one of the most stable metal oxides. There are similarities between the conversion reactions using TMA and thermite reactions. TMA assumes the role of metallic aluminum that is commonly employed in thermite reactions.[48]

The conversion-etch mechanism may be very useful in thermal ALE. For example, the conversion reaction with TMA can convert metal oxides that may not have accessible etching pathways to Al_2O_3. The conversion reaction with TMA may also convert metal oxides that have volatile fluorides and would not display self-limiting fluorination, to Al_2O_3. Al_2O_3 can then be etched by a variety of fluorine precursors, such as HF and SF_4, and metal precursors, such as $Sn(acac)_2$, $Al(CH_3)_3$, and $AlCl(CH_3)_2$.[16−18,20] Other metal precursors could also convert metal oxides to different metal oxides in addition to Al_2O_3. Moreover, metal precursors can also convert metal nitrides to more stable metal nitrides. The conversion reaction with TMA can convert metal nitrides that may not have etching pathways to AlN. AlN can be etched using sequential HF and $Sn(acac)_2$ exposures.[21]

The utility of the conversion-etch mechanism can be illustrated by examining the predicted thermochemistry of TMA reactions with a variety of metal compounds. Table 1 lists

Table 1. ΔG Values at 200°C for Various Conversion Reactions with $Al(CH_3)_3$

conversion reaction	ΔG (kcal)
$3ZnO + 2Al(CH_3)_3 \rightarrow Al_2O_3 + 3Zn(CH_3)_2$	−164.7
$1.5SiO_2 + 2Al(CH_3)_3 \rightarrow Al_2O_3 + 1.5Si(CH_3)_4$	−200.0
$1.5SnO_2 + 2Al(CH_3)_3 \rightarrow Al_2O_3 + 1.5Sn(CH_3)_2$	−229.2
$In_2O_3 + 2Al(CH_3)_3 \rightarrow Al_2O_3 + 2In(CH_3)_3$	−317.6
$Si_3N_4 + 4Al(CH_3)_3 \rightarrow 4AlN + 3Si(CH_3)_4$	−362.6

ΔG values at 200 °C for possible conversion reactions between TMA and a range of metal oxides and one metal nitride.[34] These conversion reactions depend on the existence of stable metal alkyl reaction products. A wider range of conversion reactions is possible using $AlCl_3$ instead of TMA because many metal chlorides are stable. However, the ΔG values for the $AlCl_3$ reactions are not as favorable as the ΔG values for the TMA reactions.[34]

IV. CONCLUSIONS

The atomic layer etching (ALE) of crystalline ZnO was demonstrated between 205 and 295 °C using sequential HF and TMA exposures. *In situ* quartz crystal microbalance (QCM) measurements on ZnO ALD films determined that the sequential exposures produced a linear mass loss versus time. At 265 °C, the mass changes during the HF and TMA exposures were ΔM_{HF} = +53 ng/cm^2 and ΔM_{TMA} = −172 ng/cm^2. The mass change during the TMA exposures was much larger than expected and indicated that alternative reaction pathways were occurring in addition to the ligand-exchange reaction. The average mass change per cycle (MCPC) was −119 ng/cm^2. The QCM measurements also determined that the HF and TMA reactions were self-limiting versus precursor exposure time. *Ex situ* SE measurements examined ZnO ALE for ZnO ALD films on Si(100) wafers. The ZnO ALE etch rates varied from 0.01 Å/cycle at 205 °C to 2.19 Å/cycle at 295 °C. Atomic force microscopy (AFM) measurements determined that the ZnO ALD films were smoothed by ZnO ALE.

The large mass changes during the TMA exposures suggested that the reaction mechanism of ZnO ALE follows a "conversion-etch" mechanism where a ZnO surface layer is converted to Al_2O_3 by reaction with TMA. This reaction proceeds as $3ZnO + 2Al(CH_3)_3 \rightarrow Al_2O_3 + 3Zn(CH_3)_2$. The Al_2O_3 then undergoes fluorination and ligand-exchange according to the reaction $Al_2O_3 + 4Al(CH_3)_3 + 6HF \rightarrow 6AlF(CH_3)_2 + 3H_2O$. HF fluorinates the Al_2O_3 layer to produce AlF_3. The TMA ligand-exchange transmetalation reaction then removes the AlF_3 by forming volatile $AlF(CH_3)_2$. After the AlF_3 removal, TMA then reacts with additional ZnO to regenerate the Al_2O_3 surface layer. Conversion reactions may occur frequently during the thermal ALE of other materials. The conversion-etch mechanism may enlarge the spectrum of metal compounds that can be etched using thermal ALE techniques.

AUTHOR INFORMATION

ORCID

Steven M. George: 0000-0003-0253-9184

Notes

The authors declare no competing financial interest.

ACKNOWLEDGMENTS

This research was funded by the National Science Foundation (CHE-1306131 and CHE-1609554). The authors would like to thank Dr. Huaxing Sun for the XPS elemental analysis. The authors acknowledge Dr. Amy Marquardt for the AFM surface roughness measurements and additionally thank Ms. Jasmine Wallas and Ms. Jaclyn Sprenger for the XRR and XRD measurements.

REFERENCES

(1) George, S. M. Atomic Layer Deposition: An Overview. *Chem. Rev.* **2010**, *110*, 111−131.

(2) Kanarik, K. J.; Lill, T.; Hudson, E. A.; Sriraman, S.; Tan, S.; Marks, J.; Vahedi, V.; Gottscho, R. A. Overview of Atomic Layer Etching in the Semiconductor Industry. *J. Vac. Sci. Technol., A* **2015**, *33*, 020802.

(3) George, S. M.; Lee, Y. Prospects for Thermal Atomic Layer Etching Using Sequential, Self-Limiting Fluorination and Ligand-Exchange Reactions. *ACS Nano* **2016**, *10*, 4889−4894.

(4) Agarwal, A.; Kushner, M. J. Plasma Atomic Layer Etching Using Conventional Plasma Equipment. *J. Vac. Sci. Technol., A* **2009**, *27*, 37−50.

(5) Oehrlein, G. S.; Metzler, D.; Li, C. Atomic Layer Etching at the Tipping Point: An Overview. *ECS J. Solid State Sci. Technol.* **2015**, *4*, N5041−N5053.

(6) Athavale, S. D.; Economou, D. J. Realization of Atomic Layer Etching of Silicon. *J. Vac. Sci. Technol., B: Microelectron. Process. Phenom.* **1996**, *14*, 3702−3705.

(7) Park, S. D.; Lee, D. H.; Yeom, G. Y. Atomic Layer Etching of Si(100) and Si(111) Using Cl_2 and Ar Neutral Beam. *Electrochem. Solid-State Lett.* **2005**, *8*, C106−C109.

(8) Sugiyama, T.; Matsuura, T.; Murota, J. Atomic-Layer Etching of Ge Using an Ultraclean ECR Plasma. *Appl. Surf. Sci.* **1997**, *112*, 187−190.

(9) Lim, W. S.; Park, S. D.; Park, B. J.; Yeom, G. Y. Atomic Layer Etching of (100)/(111) GaAs with Chlorine and Low Angle Forward

DOI: 10.1021/acs.chemmater.6b04529
Chem. Mater. 2017, 29, 1183−1191

Reflected Ne Neutral Beam. *Surf. Coat. Technol.* **2008**, *202*, 5701−5704.
(10) Park, S. D.; Oh, C. K.; Bae, J. W.; Yeom, G. Y.; Kim, T. W.; Song, J. I.; Jang, J. H. Atomic Layer Etching of InP Using a Low Angle Forward Reflected Ne Neutral Beam. *Appl. Phys. Lett.* **2006**, *89*, 043109.
(11) Metzler, D.; Bruce, R. L.; Engelmann, S.; Joseph, E. A.; Oehrlein, G. S. Fluorocarbon Assisted Atomic Layer Etching of SiO_2 using Cyclic Ar/C_4F_8 Plasma. *J. Vac. Sci. Technol., A* **2014**, *32*, 020603.
(12) Min, K. S.; Kang, S. H.; Kim, J. K.; Jhon, Y. I.; Jhon, M. S.; Yeom, G. Y. Atomic Layer Etching of Al_2O_3 Using BCl_3/Ar for the Interface Passivation Layer of III-V MOS Devices. *Microelectron. Eng.* **2013**, *110*, 457−460.
(13) Park, J. B.; Lim, W. S.; Park, B. J.; Park, I. H.; Kim, Y. W.; Yeom, G. Y. Atomic Layer Etching of Ultra-Thin HfO_2 Film for Gate Oxide in MOSFET Devices. *J. Phys. D: Appl. Phys.* **2009**, *42*, 055202.
(14) Kim, Y. Y.; Lim, W. S.; Park, J. B.; Yeom, G. Y. Layer by Layer Etching of the Highly Oriented Pyrolythic Graphite by Using Atomic Layer Etching. *J. Electrochem. Soc.* **2011**, *158*, D710−D714.
(15) Vogli, E.; Metzler, D.; Oehrlein, G. S. Feasibility of Atomic Layer Etching of Polymer Material Based on Sequential O_2 Exposure and Ar Low-Pressure Plasma-Etching. *Appl. Phys. Lett.* **2013**, *102*, 253105.
(16) Lee, Y.; DuMont, J. W.; George, S. M. Mechanism of Thermal Al_2O_3 Atomic Layer Etching Using Sequential Reactions with $Sn(acac)_2$ and HF. *Chem. Mater.* **2015**, *27*, 3648−3657.
(17) Lee, Y.; DuMont, J. W.; George, S. M. Trimethylaluminum as the Metal Precursor for the Atomic Layer Etching of Al_2O_3 Using Sequential, Self-Limiting Thermal Reactions. *Chem. Mater.* **2016**, *28*, 2994−3003.
(18) Lee, Y.; George, S. M. Atomic Layer Etching of Al_2O_3 Using Sequential, Self-Limiting Thermal Reactions with $Sn(acac)_2$ and HF. *ACS Nano* **2015**, *9*, 2061−2070.
(19) Lee, Y.; DuMont, J. W.; George, S. M. Atomic Layer Etching of HfO_2 Using Sequential, Self-Limiting Thermal Reactions with $Sn(acac)_2$ and HF. *ECS J. Solid State Sci. Technol.* **2015**, *4*, N5013−N5022.
(20) Lee, Y.; Huffman, C.; George, S. M. Selectivity in Thermal Atomic Layer Etching Using Sequential, Self-Limiting Fluorination and Ligand-Exchange Reactions. *Chem. Mater.* **2016**, *28*, 7657−7665.
(21) Johnson, N. R.; Sun, H.; Sharma, K.; George, S. M. Thermal Atomic Layer Etching of Crystalline Aluminum Nitride Using Sequential, Self-Limiting Hydrogen Fluoride and $Sn(acac)_2$ Reactions and Enhancement by H_2 and Ar Plasmas. *J. Vac. Sci. Technol., A* **2016**, *34*, 050603.
(22) Lee, Y.; George, S. M. Atomic layer etching of Al_2O_3 using sequential, self-limiting thermal reactions with $Sn(acac)_2$ and hydrogen fluoride. *ACS Nano* **2015**, *9*, 2061−2070.
(23) Osakada, K. Tranmetalation. In *Fundamentals of Molecular Catalysis, Current Methods in Inorganic Chemistry*, Vol. 3; Kurosawa, H., Yamamoto, A., Eds.; Elsevier Science: Amsterdam, 2003.
(24) Pearton, S. J.; Norton, D. P.; Ip, K.; Heo, Y. W.; Steiner, T. Recent Progress in Processing and Properties of ZnO. *Prog. Mater. Sci.* **2005**, *50*, 293−340.
(25) Bae, J. W.; Jeong, C. H.; Kim, H. K.; Kim, K. K.; Cho, N. G.; Seong, T. Y.; Park, S. J.; Adesida, I.; Yeom, G. Y. High-rate Dry Etching of ZnO in $BCl_3/CH_4/H_2$ Plasmas. *Jpn. J. Appl. Phys., Part 2* **2003**, *42*, L535−L537.
(26) Lee, J. M.; Chang, K. M.; Kim, K. K.; Choi, W. K.; Park, S. J. Dry Etching of ZnO Using an Inductively Coupled Plasma. *J. Electrochem. Soc.* **2001**, *148*, G1−G3.
(27) Park, J. S.; Park, H. J.; Hahn, Y. B.; Yi, G. C.; Yoshikawa, A. Dry Etching of ZnO Films and Plasma-Induced Damage to Optical Properties. *J. Vac. Sci. Technol., B: Microelectron. Process. Phenom.* **2003**, *21*, 800−803.
(28) Elam, J. W.; Groner, M. D.; George, S. M. Viscous Flow Reactor with Quartz Crystal Microbalance for Thin Film Growth by Atomic Layer Deposition. *Rev. Sci. Instrum.* **2002**, *73*, 2981−2987.
(29) Elam, J. W.; George, S. M. Growth of ZnO/Al_2O_3 Alloy Films Using Atomic Layer Deposition Techniques. *Chem. Mater.* **2003**, *15*, 1020−1028.
(30) Lee, Y.; DuMont, J. W.; Cavanagh, A. S.; George, S. M. Atomic Layer Deposition of AlF_3 Using Trimethylaluminum and Hydrogen Fluoride. *J. Phys. Chem. C* **2015**, *119*, 14185−14194.
(31) Necas, D.; Klapetek, P. Gwyddion: An Open-Source Software for SPM Data Analysis. *Cent. Eur. J. Phys.* **2012**, *10*, 181−188.
(32) Schulz, H.; Thiemann, K. H. Structure Parameters and Polarity of the Wurtzite Type Compounds SiC-2H and ZnO. *Solid State Commun.* **1979**, *32*, 783−785.
(33) Iqbal, J.; Jilani, A.; Ziaul Hassan, P. M.; Rafique, S.; Jafer, R.; Alghamdi, A. A. ALD Grown Nanostructured ZnO Thin Films: Effect of Substrate Temperature on Thickness and Energy Band Gap. *J. King Saud Univ., Sci.* **2016**, *28*, 347−354.
(34) *HSC Chemistry*; Version 5.1; Outokumpu Research Oy: Pori, Finland.
(35) Haynes, W. M., Ed.-in-Chief; *CRC Handbook of Chemistry and Physics*, 96th ed.; CRC Press, LLC: Boca Raton, FL, 2015.
(36) Lau, C. K.; Tiku, S. K.; Lakin, K. M. Growth of Epitaxial ZnO Thin Films by Organometallic Chemical Vapor Deposition. *J. Electrochem. Soc.* **1980**, *127*, 1843−1847.
(37) Elam, J. W.; Libera, J. A.; Pellin, M. J.; Stair, P. C. Spatially Controlled Atomic Layer Deposition in Porous Materials. *Appl. Phys. Lett.* **2007**, *91*, 243105.
(38) Na, J. S.; Peng, Q.; Scarel, G.; Parsons, G. N. Role of Gas Doping Sequence in Surface Reactions and Dopant Incorporation during Atomic Layer Deposition of Al-Doped ZnO. *Chem. Mater.* **2009**, *21*, 5585−5593.
(39) Graham, M. J.; Cohen, M. On the Mechanism of Low Temperature Oxidation (23−450 C) of Polycrystalline Nickel. *J. Electrochem. Soc.* **1972**, *119*, 879−882.
(40) Song, S.; Placido, F. Investigation on Initial Oxidation Kinetics of Al, Ni, and Hf Metal Film Surfaces. *Chin. Opt. Lett.* **2010**, *8*, 87−90.
(41) Derrie, J.; Commandre, M. SiO_2 Ultra Thin Film Growth Kinetics as Investigated by Surface Techniques. *Surf. Sci.* **1982**, *118*, 32−46.
(42) Fehlner, F. P. Formation of Ultrathin Oxide Films on Silicon. *J. Electrochem. Soc.* **1972**, *119*, 1723−1727.
(43) Xu, C. H.; Gao, W. Pilling-Bedworth Ratio for Oxidation of Alloys. *Mater. Res. Innovations* **2000**, *3*, 231−235.
(44) Nelson, J. C.; Oriani, R. A. Stress Generation During Anodic-Oxidation of Titanium and Aluminum. *Corros. Sci.* **1993**, *34*, 307−326.
(45) Elam, J. W.; Sechrist, Z. A.; George, S. M. ZnO/Al_2O_3 Nanolaminates Fabricated by Atomic Layer Deposition: Growth and Surface Roughness Measurements. *Thin Solid Films* **2002**, *414*, 43−55.
(46) Elam, J. W.; Routkevitch, D.; George, S. M. Properties of ZnO/Al_2O_3 Alloy Films Grown Using Atomic Layer Deposition Techniques. *J. Electrochem. Soc.* **2003**, *150*, G339−G347.
(47) Groner, M. D.; Fabreguette, F. H.; Elam, J. W.; George, S. M. Low-Temperature Al_2O_3 Atomic Layer Deposition. *Chem. Mater.* **2004**, *16*, 639−645.
(48) Wang, L. L.; Munir, Z. A.; Maximov, Y. M. Thermite Reactions - Their Utilization in the Synthesis and Processing of Materials. *J. Mater. Sci.* **1993**, *28*, 3693−3708.

DOI: 10.1021/acs.chemmater.6b04529
Chem. Mater. 2017, 29, 1183−1191